processes

MDPI

Article

A Three-Phase Relative Permeability Model for Heavy Oil Emulsion System

Zezheng Sun [1], Kang Zhou [2] and Yuan Di [1,*]

[1] College of Engineering, Peking University, Beijing 100871, China; coronation@pku.edu.cn
[2] College of Energy and Mining Engineering, Shandong University of Science and Technology, Qingdao 266590, China; zhoukang_upc@163.com
* Correspondence: diyuan@mech.pku.edu.cn; Tel.: +86-13552709129

Abstract: Chemical flooding is important and effective enhanced oil recovery processes are applied to improve the recovery of heavy oil reservoirs. Emulsification occurs during chemical flooding processes, forming an oil-in-water (O/W) emulsion system. In this work, the heavy oil emulsion system is characterized as a three-phase (continuous oil phase, dispersed oil phase, and continuous water phase) system. Based on a capillary tube model, a new relative permeability model is proposed to describe the flow of the emulsion system in porous media quantitatively, considering the physico-chemical properties of emulsions and the properties of porous media. A resistance factor is derived in this model to describe the additional resistance to the emulsion flow caused by the interaction between dispersed oil droplets and the pore system. Three dimensionless numbers related to the emulsion porous flow process were proposed and their different effects on the three-phase relative permeability are investigated. To validate the reliability of the proposed model, a one-dimensional O/W emulsion–oil displacement experiment is simulated. The maximum absolute error between the simulated results and experimental data is no more than 10%, and the new model can be used to describe the flow behavior of heavy oil emulsions in porous media.

Keywords: emulsion; chemical flood; relative permeability; enhanced oil recovery; dispersed system; porous flow

Citation: Sun, Z.; Zhou, K.; Di, Y. A Three-Phase Relative Permeability Model for Heavy Oil Emulsion System. *Processes* **2023**, *11*, 1247. https://doi.org/10.3390/pr11041247

Academic Editor: Qingbang Meng

Received: 20 March 2023
Revised: 7 April 2023
Accepted: 15 April 2023
Published: 18 April 2023

1. Introduction

Heavy oil, of which the viscosity ranges from 10^2 mPa·s to 10^4 mPa·s, has become a prominent class of unconventional oil resources [1]. Recent studies estimate that the total amount of recoverable heavy oil is almost the same as the remaining conventional oil resources [2–4]. Chemical flooding is now widely applied for enhanced heavy oil recovery [5–9], and presents several advantages in mature oilfields [10]. With the presence of chemicals such as surfactants or alkalis acting as emulsifiers, oil-in-water (O/W) emulsions could form in heavy oil reservoirs, carrying out trapping oil [5,7,11,12]. O/W emulsion is a heterogeneous system, with small oil droplets (with a size of 0.5 μm to 50 μm) dispersed in the continuous water phase. As a dispersed system, the motion of oil-in-water emulsion through the porous medium is significantly different from that of a continuous oil phase or water phase. Thus, the understanding of emulsion flow through a porous medium is crucial for the usage of a chemical flood in heavy oil reservoirs.

Many investigations on O/W emulsion porous flow have been performed through laboratory methods. Uzoigwe and Marsden pioneered the experiments on O/W emulsion flow through glass bead packing models to study the flow behavior of emulsions in porous media [13]. McAuliffe was the first to recognize the obstructive effect of emulsion droplets on fluid flow in porous media and applied this mechanism to enhance oil recovery [14]. He suggested that when an emulsion passes through porous media, the Jamin effect is particularly prominent if the oil droplet size is larger than the pore throat diameter, subsequently leading to flow limitation due to capillary resistance. However, the explanation

does not accommodate cases where the oil droplet size is smaller than the pore throat diameter. Further experiments conducted by Soo et al. proposed that, during the flow of emulsions through porous media, dispersed phase droplets can be captured and adsorbed by the media, resulting in reduced permeability [15]. In other experiments, Khambharatana et al. focused on emulsion rheology, concluding that the rheological behavior of emulsions in porous media is not significantly different from their behavior in viscometers [16]. Alvarado et al. suggested that emulsions can be considered non-Newtonian fluids when the volume fraction of a dispersed phase exceeds 50%, and can be otherwise regarded as Newtonian fluids [17]. Wang et al. observed an emulsion flood after a water flood through a micromodel and identified two main physical mechanisms for emulsion-enhanced oil recovery [18]. The first mechanism is altering the pressure distribution in the flow field by blocking the flow channels, thereby reducing residual oil. The second one is dispersed phase droplets exerting a pulling force on residual oil during the flow, causing the oil to deform into smaller droplets.

Many researchers have examined emulsion flow in porous media theoretically, developing a variety of theoretical models to describe their flow behavior. There are three widely recognized conventional mathematical models now: the bulk viscosity model, the retardation model, and the deep filtration model. Alvarado et al. introduced the bulk viscosity model [17], considering emulsions as homogeneous single-phase fluids. They found that the rheological properties of O/W emulsions in porous media were similar to their properties in capillaries. They concluded that when the dispersed phase ratio exceeded 50%, the emulsions could be considered non-Newtonian fluids and provided parameters to characterize their rheology. Abou-Kassem et al. further refined the bulk viscosity model by presenting a modified Darcy's law applicable to non-Newtonian emulsions [19]. However, the bulk viscosity model merely treats emulsions as single-phase fluids, similar to polymer solutions, and does not account for the interactions between dispersed phase droplets and pores. As a result, this model is only applicable in a limited range of situations.

The retardation model proposed by Devereux [20] was to explain the phenomenon of permeability reduction observed by McAuliffe. Based on the Buckley–Leverett model, he introduced a dispersion phase resistance factor to represent the capillary resistance experienced by the dispersed phase during flow. This model aligns well with the experimental results of emulsion flow in porous media but cannot predict the situation of a water injection following emulsion flow. Yu and Ding et al. [21,22] made improvements to the retardation model, considering the porous media as channels composed of larger pores and smaller pore throats and taking into account the blocking phenomenon caused by multiple emulsion droplets. The modified model can better predict the experimental phenomena of water flooding following emulsion flooding. However, the retardation model assumes the properties of emulsions are constant and cannot describe the variations of emulsion droplets during flow.

Soo et al. introduced the deep filtration theory into emulsion porous flow to consider the interaction between droplets and pore throats [23]. They assumed that dispersed phase droplets would be captured by the porous media such as tiny particles. The captured droplets would block smaller flow channels, resulting in a decrease in permeability. However, the deep filtration model assumes that once droplets are captured by pores, they cannot be remobilized, which means the reduction in permeability is irreversible. This is inconsistent with experimental observations. Although some researchers improved the model by considering the remobilization of droplets [24], the introduction of new parameters made the modified model excessively complex.

Existing models for emulsion porous flow often represent porous media as a capillary bundle with uniform diameters. They usually use the flow behavior in a single capillary as a substitute for the porous medium. However, many theoretical and experimental research studies have shown that the interaction between dispersed droplets and pores plays a significant role in affecting the flow. Wei et al. [25] studied emulsion flow in constricted capillaries using a lattice Boltzmann simulation method. They argued the

emulsion capillary flow may have complex mechanism, including deformation, snap-off, and the "trap effect". Thus, we regard the relative size of capillaries and droplets being the most critical factor in this study. Additionally, most of the models mainly focused on the single O/W emulsion porous flow process, which only includes dispersed oil and continuous water. These models are unable to describe the three phases of flow (dispersed oil, continuous water, and continuous oil) that occur during heavy oil recovery adequately. In this work, a new three-phase relative permeability model is proposed, considering the physicochemical properties of emulsions and the pore size distribution of the porous media. The interaction between the dispersed oil droplets and pore system is characterized by a resistance factor, which is carefully derived considering the various relative sizes of pores and droplets.

2. Emulsion Flow through a Single Capillary Tube

2.1. Single-Phase Flow in a Single Capillary Tube

Consider a single-phase fluid (oil or water) flowing through a straight circular capillary tube of uniform radius R and length L. Assuming the single-phase fluid is Newtonian and the flow is laminar, the Hagen–Poiseuille equation could be applied, written as:

$$\frac{dv}{dr} = -\frac{1}{2}\frac{dp}{dz} \times \frac{r}{\mu} \tag{1}$$

where μ is viscosity of the fluid, Pa·s; r is the radical coordinate, m; z is the axial coordinate, m; p is the fluid pressure, Pa; v is the velocity of fluid at a point distance r from the axis, m/s.

By integrating Equation (1) and applying the non-slip boundary condition, we have the velocity function [26]:

$$v(r) = \frac{\Delta P}{4\mu L}\left(R^2 - r^2\right) \tag{2}$$

where ΔP is the pressure drop along the tube.

Then, the flow rate of the single-phase fluid through a single capillary tube, q_0, could be derived by integrating the velocity over the tube cross section:

$$q_0 = \int_0^R v d\left(\pi r^2\right) = \frac{\Delta P}{8\mu L}\pi R^4 \tag{3}$$

2.2. Single-Phase Flow in a Single Capillary Tube

The flow of an O/W emulsion through a porous medium, as addressed previously, is significantly affected by the volume fraction of dispersed oil droplets, ϕ_d, and the relative size between dispersed oil droplets and pores. The effects of both aspects could be reflected by the behavior of the emulsion flow through a single capillary tube. We consider dispersed oil droplets in the emulsion flow as spheres of a uniform diameter d_e, m, and define the diameter ratio λ of the droplets diameter to the capillary tube diameter, written as:

$$\lambda = \frac{d_e}{2R} \tag{4}$$

The aim is to represent the total flow rate of the emulsion flow through a single capillary tube q, as a function of the pressure drop along the tube ΔP, the diameter ratio λ, and the dispersed phase volume fraction ϕ_d.

2.2.1. Case of a Line of Intermediate-Sized Spherical Droplets

We begin by considering the case that the diameter of dispersed oil droplets is quite comparable with the capillary tube diameter, where $0 \ll \lambda < 1$. In this case we assume that, as illustrated in Figure 1a, the dispersed droplets are located on the axis of the cylinder

and equally spaced. The distance between neighboring drops is βR. In dimensionless form, the equations of motion and continuity for this problem are written as follows:

$$\begin{cases} -\nabla \boldsymbol{P}' + \nabla^2 \boldsymbol{v}' = 0 \\ \nabla \cdot \boldsymbol{v}' = 0 \end{cases} \tag{5}$$

where $\boldsymbol{P}'$ and $\boldsymbol{v}'$ are dimensionless pressure and velocity, respectively.

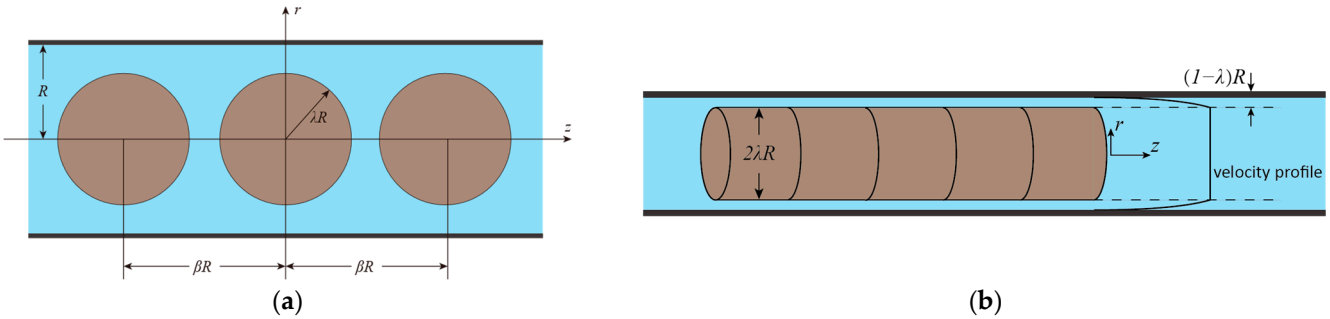

Figure 1. Schematic view of dispersed droplets with intermediate size in single capillary tube. (**a**) Dispersed droplets are located on the axis of the cylinder and equally spaced; (**b**) the simplified "stacked coins" model.

This problem is analytically investigated by Wang [27]. They gave a solution in dimensionless form that could compute the pressure drop per sphere, written as:

$$\Delta P'_{drop} = -8F_2 - 16E_2 - 4V\beta \tag{6}$$

where V is average velocity, defined as $V = \frac{q}{2\pi r^2}$; E_2 and F_2 are the first term of constant sequence E_{2s} and F_{2s}, respectively. E_{2s}, F_{2s} is used for discretization of the stream function ψ_a, written as:

$$\psi_a = \sum_{s=1}^{\infty} \left[E_{2s} \psi_{2s}^{(1)} + F_{2s} \psi_{2s}^{(2)} \right] \tag{7}$$

where $\psi_{2s}^{(i)}$ is defined as:

$$\psi_{2s}^{(i)} = \frac{1}{(2s-2)!} \frac{\partial^{2s-2} \psi^{(i)}}{\partial z^{2s-2}} \ (s \geq 1,\ i = 1,2) \tag{8}$$

Then, in dimensional form, the total pressure gradient could be written as:

$$\frac{dp_z}{dz} = \frac{\mu}{R}(-VG_V + UG_U) - \frac{4\mu V}{R^2} + \rho g \tag{9}$$

where G_V and G_U are coefficients derived from E_2 and F_2 values; U is the velocity of spheres; and μ is the viscosity of the external phase, in O/W it refers to the viscosity of water, $\mu = \mu_w$.

The analytical solution above requires excessive numerical computations for further use. To simplify the solution, further assumptions must be made. The effect of gravity could be neglected, so that term ρg could be disregarded. The zero-drag assumption is also adopted, which means that we assume the flow of the external phase fluid and dispersed droplets in the cylindrical tube is stable; thus, the external phase fluid exerts zero drag force on the dispersed droplets. Then, the velocity of the spheres U could be represented by V, reducing Equation (9) to a solvable form:

$$\frac{dp_z}{dz} = -\frac{4\mu}{R^2} V \left(1 + G_{V_0}\right) \tag{10}$$

The flow rate is addressed as:

$$q_e = \frac{1}{1 + G_{V_0}} \frac{\Delta P}{8\mu L} \pi R^4 \tag{11}$$

For a simpler "stacked coins" model, as schemed in Figure 1b, when $\beta = 2\lambda$, dispersed droplets are regarded as stacked cylinders of the same diameter with the droplets. We have the additional pressure drop coefficient:

$$G_{V_0} = \frac{\lambda^4}{1 - \lambda^4} \tag{12}$$

Here, a resistance factor ξ is defined by the ratio of single external phase Poiseuille flow rate through a capillary tube to that of the O/W emulsion flow, with the same tube length and total pressure drop, written as

$$q_e = \frac{1}{\xi} q_0 \tag{13}$$

For more general cases that dispersed droplets are not attached to each other, when $\beta > 2\lambda$, consider the tube part of length βR in the capillary as a serial connection of "stacked coins" flow part of length $2\lambda R$ and Poiseuille flow part of length $(\beta - 2\lambda)R$. Then, q_e is derived as:

$$q_e = \frac{1}{\left(1 + \frac{\lambda^4}{1-\lambda^4} \frac{2\lambda}{\beta}\right)} \frac{\Delta P}{8\mu_w L} \pi R^4 \tag{14}$$

Notice that the dispersed droplets volume faction ϕ_d could be presented by β and λ in this case:

$$\phi_d = \frac{4\lambda^3}{3\beta}, \; meanwhile \; \frac{\phi_d}{\lambda^2} < \frac{2}{3} \tag{15}$$

The resistance factor then is written as:

$$\xi(\lambda, \phi_d) = 1 + \frac{3\lambda^2 \phi_d}{2(1 - \lambda^4)} \tag{16}$$

However, a correction coefficient $G' \approx 3/4$ is suggested by Wang for G_{V_0} when using the "stacked coins" model on a line of spherical droplets [27], based on numerical results. Thus, the resistance factor after correlation becomes:

$$\xi(\lambda, \phi_d) = 1 + \frac{9\lambda^2 \phi_d}{8(1 - \lambda^4)} \tag{17}$$

2.2.2. Case of a Large Amount of Small-Sized Droplets

Now, consider the case that there is an O/W emulsion flow through a capillary tube, when the size of the droplets is relatively small and the volume faction of droplets are large, satisfying:

$$\frac{\phi_d}{\lambda^2} \geq \frac{2}{3} \tag{18}$$

As schemed in Figure 2a, we assume that the dispersed oil droplets are uniformly distributed near the axis of the tube, surrounded by a clear annulus of continuous water. The assumption is made since the reservoir is usually hydrophilic due to the impacts of surfactants during chemical flooding. Then, we consider the effective resistance of the dispersed oil droplets flowing down the center of the tube. As illustrated in Figure 2b, the suspension in the center of the tube is approximated to an axial cylindrical flow with an effective radius r_{eff}, and the width of the surrounding annulus of continuous water is $\left(R - r_{eff}\right)$.

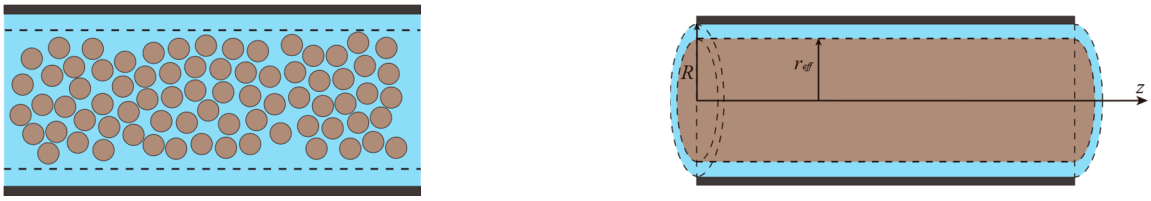

(**a**) (**b**)

Figure 2. Schematic view of a large amount of small, dispersed droplets spread in a single capillary tube. (**a**) Dispersed droplets are uniformly spread on the axis of the cylinder; (**b**) the schematic view of the effective radius.

According to the derivation by Thomas [28], the total flow rate of the tube could be written as:

$$q_e = \left(1 - \left(\frac{r_{eff}}{R}\right)^4\right) \frac{\Delta P}{8\mu_w L} \pi R^4 \tag{19}$$

where $\frac{r_{eff}}{R} = \frac{c_0}{2c - c_0}$. Here, $c_0 = \phi$ is the reservoir concentration of dispersed oil, and c is the core concentration, determined on the packing condition of dispersed droplets. If the deformation of small droplets is not considered, we could regard those dispersed oil droplets as random close packing spheres, $c \approx 0.64$.

The resistance factor in this case could then be written:

$$\xi(\phi_d) = \frac{1}{1 - \left(\frac{\phi_d}{1.28 - \phi_d}\right)^4} \tag{20}$$

where ϕ_d is no more than 0.64.

2.2.3. Case of Deformed Large-Sized Droplets

When $\lambda > 1$, the size of droplets is larger than that of the capillary tube, and the deformation of droplets is considered. As illustrated in Figure 3, the shape of the spherical droplets became a long cylindrical shape with caps when entering the smaller cylindrical tube. The long drop is slowly moving relative to the tube walls with a steady velocity U. The oil drop is surrounded by a thin water film of uniform thickness $b = \epsilon R$, since the reservoir is considered hydrophilic.

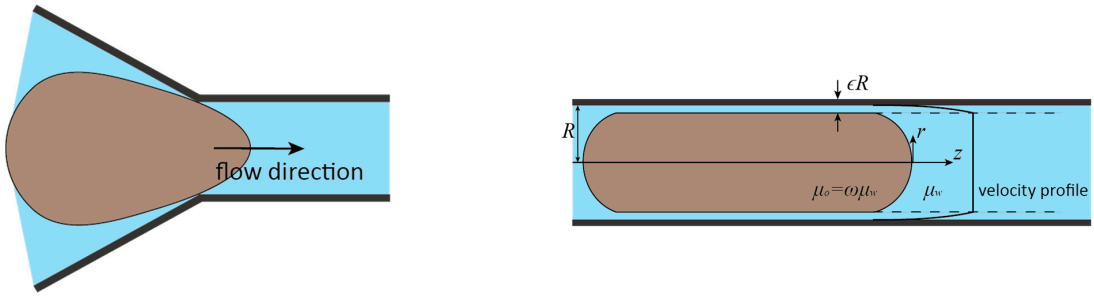

(**a**) (**b**)

Figure 3. Schematic view of a deformed droplet with larger diameter than the capillary. (**a**) The schematic view of the droplet deforming to enter a smaller capillary; (**b**) the schematic view of the deformed droplet in the capillary.

By performing an analytical investigation on the front profile of the long drop, Hodges suggested that the film thickness ϵ can be predicted as a function of capillary number Ca and viscosity ratio ω. It is written as [29]:

$$\epsilon = F(\omega, Ca) Ca^{\frac{2}{3}} \tag{21}$$

In Equation (19), the value of $F(\omega, Ca)$ is determined by following:

$$\begin{cases} F = F_0 \approx 1.337,\ \omega \ll \epsilon^{-\frac{1}{2}} \\ F = 2^{\frac{2}{3}} F_0 \approx 2.123,\ \epsilon^{-\frac{1}{2}} \ll \omega \ll \epsilon^{-1} \\ F = 4^{\frac{2}{3}} F_0 \approx 3.370,\ \omega \gg \epsilon^{-1} \\ F \approx 2^{\frac{2}{3}} F_0 \left(2 + 4\omega Ca^{\frac{2}{3}} F\right) / \left(1 + 4\omega Ca^{\frac{2}{3}} F\right),\ \omega \sim \epsilon^{-1} \end{cases} \tag{22}$$

where viscosity ratio ω is defined as $\omega = \frac{\mu_o}{\mu_w}$; capillary number Ca is defined as $Ca = \frac{\mu_w U}{\sigma}$, and σ is the interfacial tension between oil and water; F_0 is a unique solution for the Landau–Levich equation:

$$h_{x'x'x'} h^3 + 1 - h = 0 \tag{23}$$

where $x' = 3^{\frac{1}{3}} F^{-\frac{1}{2}} x$.

As for the circumstance $\omega \sim \epsilon^{-\frac{1}{2}}$, F is the solution for equation:

$$h_{x'x'x'} h^3 + 2(1 - h) + v_b h = 0 \tag{24}$$

where $x' = 6^{\frac{1}{3}} F^{-\frac{1}{2}} x$ and v_b is the relative velocity between different zones of drop interface.

Regarding the motion of the thin film as the Couette flow, we could also apply the serial connected stacked-coins model for this case. If the long oil drop is considered cylindrical when measuring its volume, the total flow rate of the tube could then be written as:

$$q_e = \frac{1}{\left(1 + \frac{\phi_d (1-\epsilon)^2}{1-(1-\epsilon)^4}\right)} \frac{\Delta P}{8\mu_w L} \pi R^4 \tag{25}$$

Thus, in this case ξ could be written as:

$$\xi(\epsilon, \phi_d) = 1 + \frac{\phi_d (1-\epsilon)^2}{1-(1-\epsilon)^4} \tag{26}$$

3. Relative Permeability Model and Pore Size Distribution Function

3.1. Relative Permeability Based on Capillary Bundle Model

Now we investigate the O/W emulsion flow through a porous medium. Here, the porous medium is simplified to a bundle of capillary tubes, as shown in Figure 4a. These capillary tubes are assumed to possess the same length L, but with different diameters, as we know the size of pores plays an important role in the process. The size and the amount of the capillary tube could be determined by the pore size distribution (PSD) function $f(R)$. $f(R)$ is defined as the relative abundance of each pore radii R in a representative volume of porous medium, satisfying:

$$\int_0^\infty f(R) dR = 1 \tag{27}$$

The permeability K and porosity ϕ of the proposed model shall be the same with that of the porous medium. For a single-phase flow in porous media, from Equation (3) the total flow rate of all tubes could be written as:

$$Q = \frac{\phi A \Delta P}{8\mu L} \int_0^\infty R^2 f(R) dR \tag{28}$$

where A is the cross-section of the porous medium. By Darcy's law, we have:

$$Q = \frac{KA\Delta P}{\mu L} \tag{29}$$

Combining Equations (28) and (29), the relationship between permeability and porosity could be expressed by the PSD function:

$$K = \frac{\phi}{8} \int_0^\infty R^2 f(R) dR \tag{30}$$

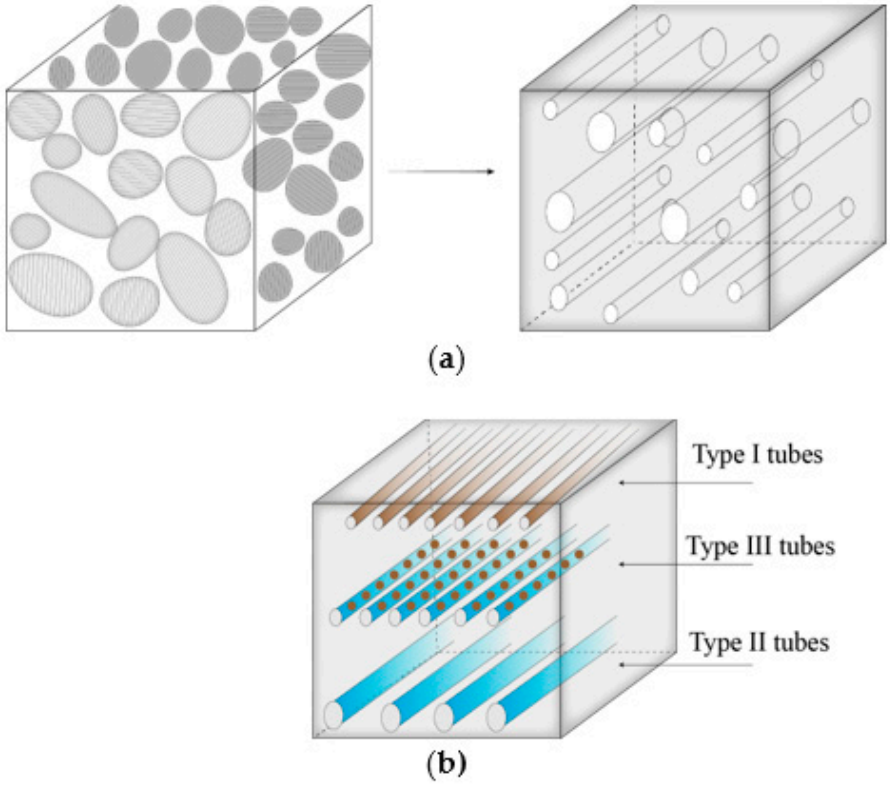

Figure 4. Schematic view of the porous medium and the proposed capillary bundle model. (**a**) Porous medium and capillary bundle model; (**b**) the way the capillary tubes divided into three types.

The flow of the O/W emulsion system through porous media, according to the experimental study, can usually be divided into three flowing zones. That is, the oil flowing zone, the water flowing zone, and the O/W emulsion flowing zone. The oil flowing zone is characterized by the flow of the continuous oil phase, and the water flowing zone is characterized by the flow of the continuous water phase. The emulsion flowing zone is characterized by the flow of both the dispersed oil phase and continuous water phase. Assume that no further dispersion of oil phase take place, and the distribution of dispersed oil droplets does not become more homogeneous in the continuous water phase during the flow.

As shown in Figure 4b, the capillary tubes of the proposed model are divided into three types based on their size, corresponding to the flowing zones:

Type I: Smaller tubes. Since the chemical flooding treatment is usually used after the water flooding, and for heavy oil reservoir the viscosity of oil is much larger than water, we think the water phase is more likely to flow down the larger tubes, and the smaller tubes are totally occupied by the continuous oil phase. Type I tubes refer to the oil flowing zone.

Type II: Larger tubes. The larger tubes are occupied by the continuous water phase. Type II tubes refer to the water flowing zone.

Type III: Intermediate-sized tubes. During the chemical flooding procedure, surfactant is present to alter the wettability of the porous medium (mostly from hydrophobic to hydrophilic), allowing water to enter some oil-occupied channels, so that the O/W emulsion could form. In the proposed model, we regard the intermediate-sized tubes occupied by

the O/W emulsion composed by the continuous water phase and dispersed oil phase, referring to the emulsion flowing zone.

Let the radii of the Type I tubes be $0 < R \leq R_1$, the radii of Type II tubes be $R_2 < R < \infty$, and the radii of Type III tubes be $R_1 < R \leq R_2$. The total flow rate of three types of tubes could then be written as:

$$Q_I = \frac{\phi A \Delta P}{8\mu_o L} \int_0^{R_1} R^2 f(R) dR \tag{31}$$

$$Q_{II} = \frac{\phi A \Delta P}{8\mu_w L} \int_{R_2}^{\infty} R^2 f(R) dR \tag{32}$$

$$Q_{III} = \frac{\phi A \Delta P}{8\mu_w L} \int_{R_1}^{R_2} \frac{1}{\xi(\lambda, \phi_d, \epsilon)} R^2 f(R) dR \tag{33}$$

where Q_I is the total flow rate of Type I tubes; Q_{II} is the total flow rate of Type II tubes; Q_{III} is the total flow rate of Type III tubes; and the value of ξ is calculated by Equations (17), (20) and (26).

By Darcy's law of multiphase flow:

$$Q_i = \frac{K K_{ri}}{\mu_i} A \nabla P \tag{34}$$

where K_{ri} is the relative permeability of phase i, μ_i is the viscosity of phase i.

It is noted that the viscosity of the dispersed oil phase is regarded the same as the viscosity of water μ_w, as the external phase of the O/W emulsion is water. Then, by Equations (30)–(33), the relative permeability of each phase is written as follows:

$$K_{ro} = \int_0^{R_1} R^2 f(R) dR / \int_0^{\infty} R^2 f(R) dR \tag{35}$$

$$K_{rw} = \int_{R_2}^{\infty} R^2 f(R) dR / \int_0^{\infty} R^2 f(R) dR + (1 - \phi_d) \int_{R_1}^{R_2} \frac{R^2 f(R)}{\xi(\lambda, \phi_d, \epsilon)} dR / \int_0^{\infty} R^2 f(R) dR \tag{36}$$

$$K_{rdo} = \phi_d \int_{R_1}^{R_2} \frac{R^2 f(R)}{\xi(\lambda, \phi_d, \epsilon)} dR / \int_0^{\infty} R^2 f(R) dR \tag{37}$$

where K_{ro} is the permeability of the continuous oil phase; K_{rw} is the permeability of the continuous water phase; and K_{rdo} is the permeability of dispersed oil phase.

To be noted, the saturation of each phase could be calculated as follows:

$$S_o = \int_0^{R_1} f(R) dR \tag{38}$$

$$S_w = \int_{R_2}^{\infty} f(R) dR + (1 - \phi_d) \int_{R_1}^{R_2} f(R) dR \tag{39}$$

$$S_{do} = \phi_d \int_{R_1}^{R_2} f(R) dR \tag{40}$$

where S_o, S_w, and S_{do} are the saturation of the continuous oil phase, continuous water phase, and dispersed oil phase, respectively.

In practice, the PSD function $f(R)$ could be converted from the capillary pressure curve $P_c = P_c(S_w)$, based on the Washburn equation:

$$P_c = \frac{2\sigma_0 cos\theta}{R} \tag{41}$$

where σ_0 is the interfacial tension and θ is the contact angle between the non-wetting phase and the pore walls.

3.2. PSD Functions

To analyze the effects of different parameters on the relative permeability curves of the heavy oil O/W emulsion system, we must choose appropriate PSD functions. The power law distribution function and the log-normal pore size distribution function are applied, since both are the most commonly used PSD functions [30–32].

The power law pore size distribution function is written as:

$$f(R) = (n+1)\frac{R^n}{R_{max}^{n+1} - R_{min}^{n+1}} \tag{42}$$

where R_{max}, R_{min} are the supposed largest and smallest radius of the pores, respectively, and n is the power law exponent.

The log-normal pore size distribution function is written as:

$$f(R) = \frac{1}{R\sqrt{2\pi\alpha}} e^{-\log\left(\frac{R}{\overline{R}} + \frac{\alpha}{2}\right)/2\alpha} \tag{43}$$

where $\alpha = log\left(1 + \left(\frac{\sigma}{\overline{R}}\right)^2\right)$; σ is the standard deviation and $\overline{R}$ is the mean radius.

For the power law PSD function, set the value of n as $-3/4$, $-1/2$, $-1/4$, 0, $1/4$, $1/2$, and $3/4$. R_{max} is assumed to be a hundred times larger than R_{min}. Then, the power law PSD curves are generated as shown in Figure 5a.

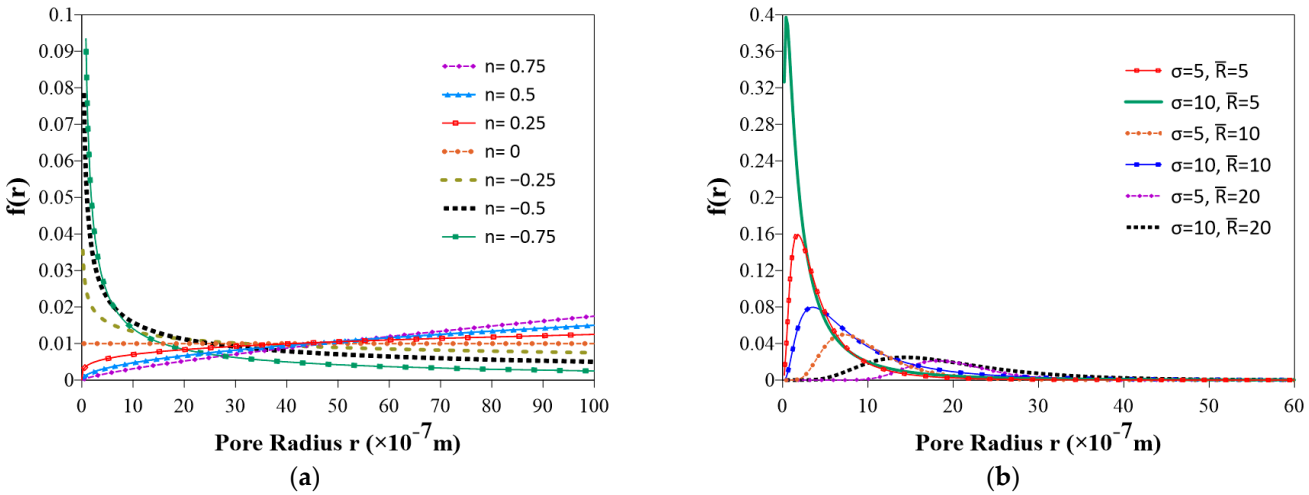

Figure 5. Different PSD function curves. (**a**) Power law PSD functions, with n value of $-3/4$, $-1/2$, $-1/4$, 0, $1/4$, $1/2$ and $3/4$; (**b**) log-normal PSD functions, with values of σ and $\overline{R}$ as 5, 5; 5, 10; 5, 20; 10, 5; 10, 10; 10, 20, respectively.

For the log-normal PSD function, set the values of σ and $\overline{R}$ as 5, 5; 5, 10; 5, 20; 10, 5; 10, 10; 10, 20, respectively. The log-normal PSD function curves are generated as shown in Figure 5b.

For the power-law PSD function, it is obvious from the figure that when n lies between 0 and -1, smaller pores constitute most of the overall pore population, with this tendency diminishing as n increases. When n equals 0, the distribution of pore sizes is uniform. Conversely, when n is greater than 0, larger pores gain prominence, and this trend amplifies as n continues to increase. For the log-normal PSD function, it could be noticed that even with the same average pore radius, different variances have a significant impact on the

peak position of the pore size distribution. A smaller σ would result in a smoother function curve, also making the peak position closer to the average pore radius.

Based on Equations (35) and (36), the oil–water relative permeability curve could then be presented as Figure 6a, with the given PSD functions. Figure 6b shows the relative permeability of the continuous oil phase and continuous water phase, when there are no emulsions participating. By analyzing the curves depicted in Figure 6, it can be observed that as the proportion of smaller-sized pores increases, the relative permeability of the water phase increases at equivalent saturation levels. Additionally, a more concentrated distribution of pore sizes results in an enhanced curvature of the relative permeability curve for the water phase. It should be noted that the wettability of different phases was not considered in the proposed model, thus the value of $K_{ro} + K_{rw}$ always equals 1.

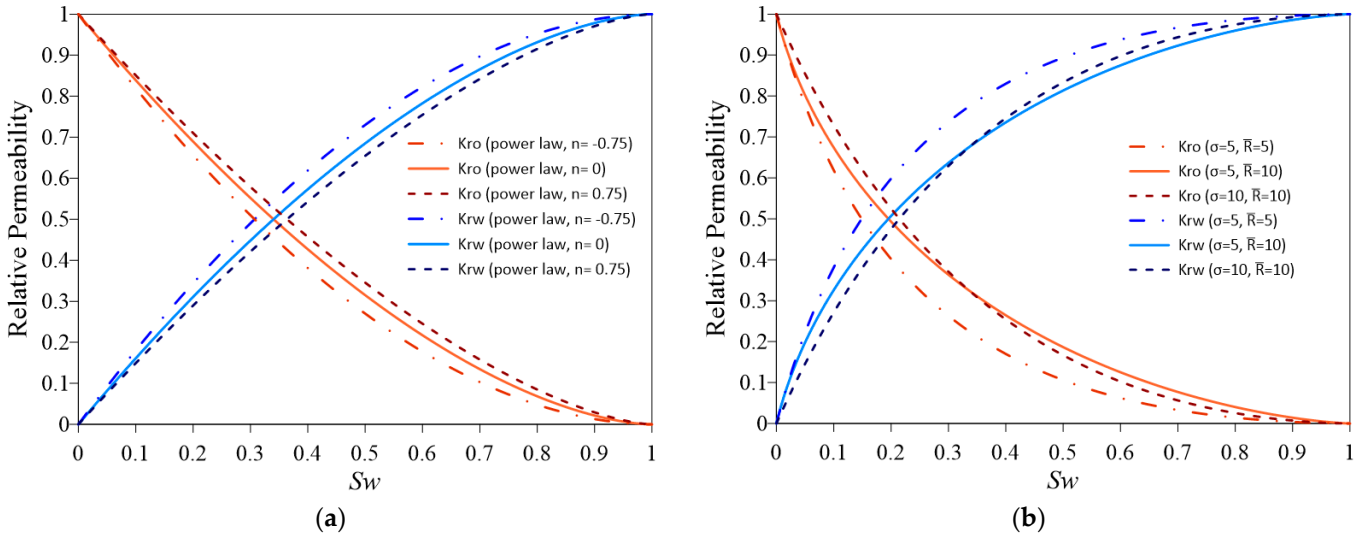

Figure 6. Oil–water relative permeability curves with different PSD functions. (**a**) Power law PSD functions; (**b**) log-normal PSD functions.

4. Experimental Validation of the Relative Permeability Model

4.1. Experimental Setups

To validate the proposed model, a one-dimensional sandpack displacement experiment has been carried out. As shown in Figure 7, the sandpack holder was packed by 100-150 mesh quartz sands, and was initially saturated with crude oil. The sandpack was then injected continuously by a prepared O/W emulsion, at a constant flow rate of 0.5 mL/min. The O/W emulsions were prepared from heavy crude oil with a viscosity of 206 mPa·s at 60 °C (same sample as the saturated oil). The surfactant used to form emulsions in this experiment is SDS with a concentration of 0.5 wt%. The dispersed oil volume fraction of the prepared O/W emulsions was 20%. The length and the diameter of the sandpack holder were 80 cm and 2.5 cm, respectively. The porosity and water permeability of the sandpack were tested before the experiment, and the values of which were 0.38 and 1890 mD, respectively. The residual oil saturation and the irreducible water saturation were also measured, with values of 0.435 and 0.125, respectively.

4.2. Numerical Simulation Using the Proposed Relative Permeability Model

In order to simulate the emulsion flooding experiment using the proposed relative permeability model, it is imperative to first compute the three-phase relative permeability curves utilized in the simulation. Therefore, it is needed to determine requisite physico-chemical parameters for the model, including: the volume faction of dispersed droplets ϕ_d, the diameter ratio of the droplets diameter to the capillary tube diameter λ, the capillary number Ca, and the pore size distribution function $f(R)$. Here, ϕ_d = 0.2 since the O/W emulsions used in the experiment is so prepared. The capillary number Ca is assumed to

be 10^{-4}, since the viscosity of oil was 206 mPa·s and the interfacial tension was around 10^{-2} mN/m with the presence of surfactants. The value of λ was determined as 1.2 based on the experimental observations. As for the PSD function of the sandpack, a log-normal PSD function was used, with a standard deviation $\sigma = 3$ and mean radius $\overline{R} = 5$, based on the characteristics of 100–150 mesh quartz sands. With the given parameters and function, the relative permeability of all three phases (continuous oil, continuous water, and dispersed oil) could then be calculated, shown as Figure 8. Notice the color bar of K_{rdo} is different from K_{ro} and K_{rw}, since the relative permeability of the dispersed oil phase is too small compared to that of the continuous water and continuous oil phase in this case. The maximum value of K_{rdo} in this case is 0.016, while K_{ro} and K_{rw} both vary from 0 to 1. It could be also noticed that the saturation of dispersed oil is always lesser than 0.2. This is because the saturation of dispersed oil is limited by the given ϕ_d, since it is the internal phase of the emulsions.

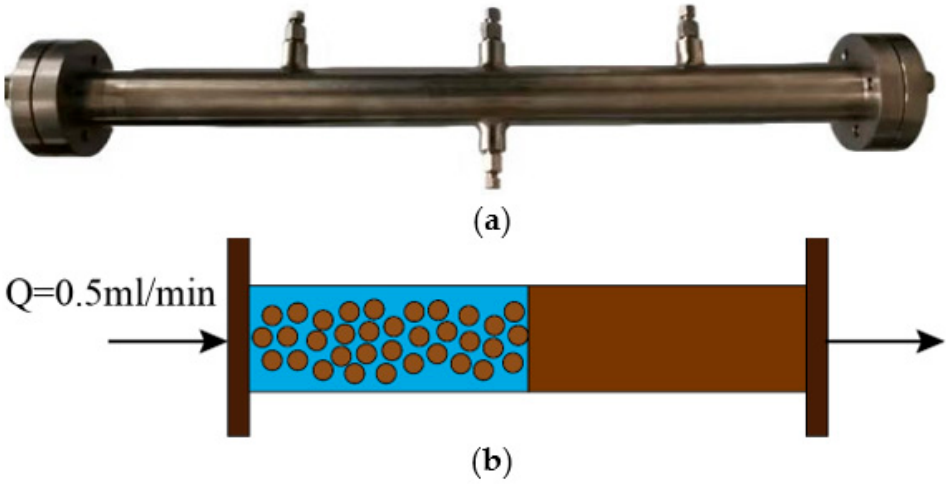

Figure 7. (**a**) Photo of the prepared sandpack. (**b**) Schematic view of the sandpack. The sandpack was initially saturated with oil, then injected by pre-prepared O/W emulsions.

The other parameters required for the simulation are consistent with those measured in the experiments, where the length of the sandpack $L = 80$ cm, and the cross area of the sandpack $A = 4.84$ cm^2. The porosity of the sandpack $\phi = 0.38$, and the permeability of the sandpack $K = 1890$ mD. The viscosity of the oil phase μ_o=206 mPa·s, and the viscosity of water $\mu_w = 1$ mPa·s. The injection was at a constant rate that $Q = 0.5$ mL/min. A one-dimensional three-phase simulator was used to simulate the whole process, the time step was set to 30 s, and the total simulation time was set to 30,000 s.

Due to experimental limitations, it is unable to quantify the volume of the dispersed oil phase in the produced emulsions. Therefore, the volumes of the continuous water phase and dispersed oil phase from the simulation results were added to compare with the cumulative production of the emulsions measured in the experiments. Since the sandpack is initially oil-saturated in this experiment, all the continuous water phase comes from the injected emulsion. Additionally, it has been experimentally verified that the dispersed oil phase in the prepared emulsion can be considered stable. Thus, the comparison between the simulation results and the experimental data is reliable. The simulation results are shown in Figure 9, compared with the experimental data. As illustrated in the figure, the simulation results and experimental data showed a considerable agreement, with the maximum error not surpassing 10%. The results validated the reliability of the proposed relative permeability model.

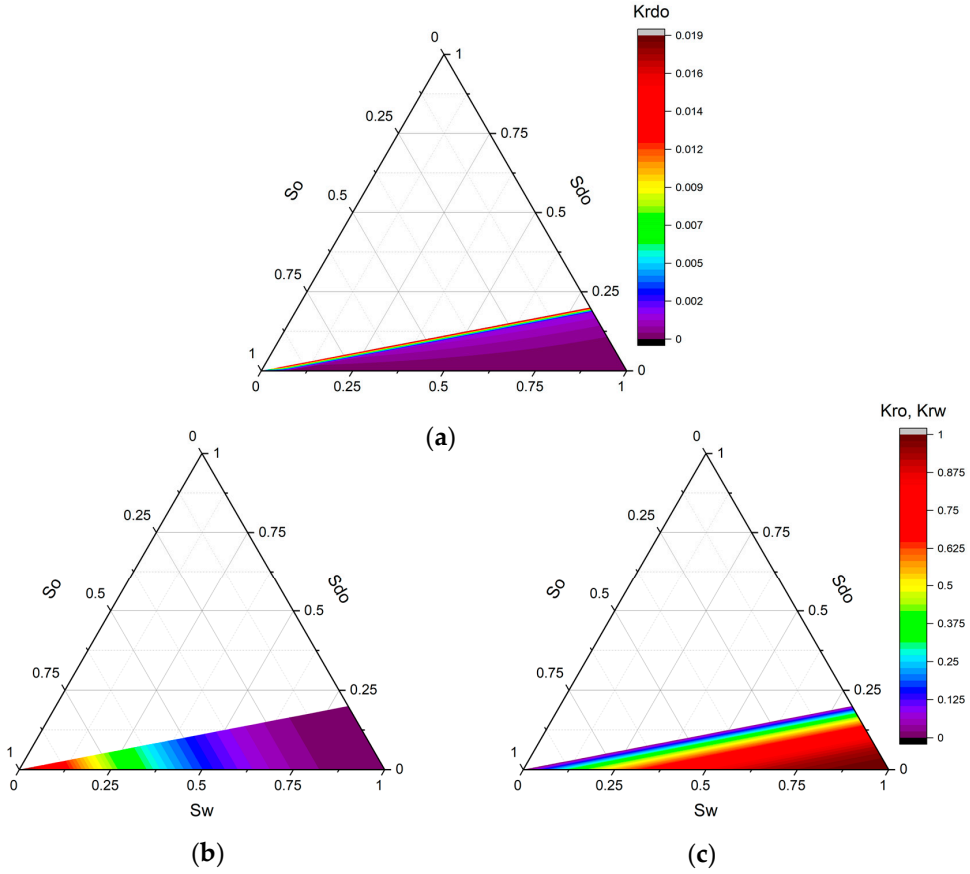

Figure 8. Three-phase permeability ternary diagram for simulation. (**a**) Permeability of dispersed oil phase; (**b**) permeability of continuous oil phase; (**c**) permeability of continuous water phase. The permeability of the continuous oil phase and continuous water phase shares the same color bar.

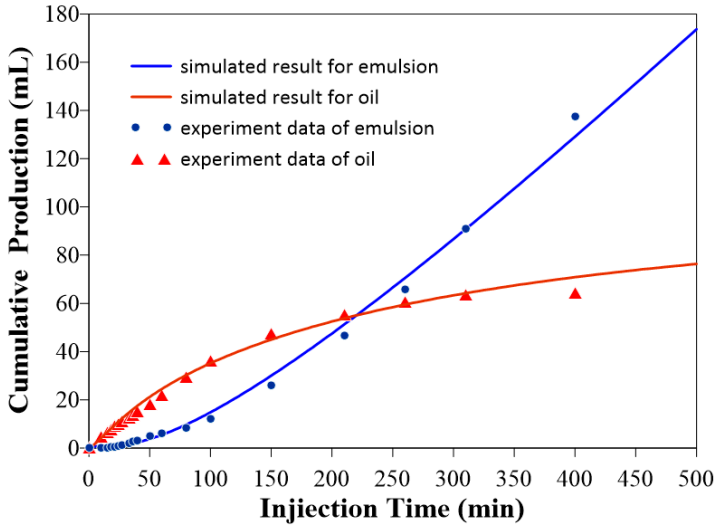

Figure 9. Comparison between simulation results and experiment data.

5. Dimensionless Parameters Analysis

To further comprehend the porous flow behavior in heavy oil emulsion systems, it is essential to examine the influence of the three dimensionless numbers ϕ_d, λ, Ca on the ternary diagram of relative permeability. Upon investigating Equations (35) and (38), it becomes apparent that, within the proposed model, the relative permeability of

the continuous oil phase is only related to its own saturation (given the PSD function). This property can be also found in Figure 8b. As the impact of the PSD function on the relative permeability of the continuous oil phase has been previously illustrated in Figure 6, the subsequent analysis will focus on the effects of the different values of the three dimensionless numbers on the continuous water phase and the dispersed oil phase.

The PSD function we choose in the following analysis is the same as the function we use in the simulation, which is a log-normal PSD function with a standard deviation $\sigma = 3$ and mean radius $\overline{R} = 5$. Figure 10 shows the relative permeability ternary diagram of the continuous water phase and dispersed oil phase, respectively, while $\phi_d = 0.4$, $\lambda = 0.9$, and $Ca = 10^{-4}$. The maximum value of K_{rdo} in Figure 10a is 0.026. Figure 11 shows the relative permeability ternary diagram of the continuous water phase and dispersed oil phase, respectively, while $\phi_d = 0.4$, $\lambda = 0.6$, and $Ca = 10^{-3}$. The maximum value of K_{rdo} in Figure 11a is 0.167. By comparing Figures 10b and 11b, it could be noticed from the contour lines that K_{rw} can be considered solely influenced by the value of S_w when the maximum value of K_{rdo} is much less than 1. However, when the value of K_{rdo} is more comparable with 1, the effect of the S_{do}. value on K_{rw} becomes more non-negligible, especially when S_w is closer to 0, the reason of which can be learned by investigating Equations (36) and (39). The value of K_{rdo} is much less than 1, means that the flow of emulsions in the pores is subject to significant resistance by the oil droplets, causing the contribution of the flow from the emulsion to the production of the continuous water phase is relatively small.

Figure 12 shows the relative permeability ternary diagrams of the dispersed oil phase when $\phi_d = 0.4$, $Ca = 10^{-4}$, and $\lambda = 0.6$, 0.9, and 1.2, respectively. The maximum values of the three K_{rdo} diagrams are 0.0374, 0.0255, and 0.0239, respectively. The effect of the value of the diameter ratio between the dispersed phase droplets and pores on the result of K_{rdo} value is apparent. This pattern could be easy to understand intuitively. As the diameter of the dispersed phase droplets approaches the size of the pores, the likelihood of the droplets becoming trapped by the pores increases, leading to substantial flow resistance. When the droplet size is statistically larger than the average pore size, this probability becomes higher, making less droplets have the chance to pass the pores during the flow.

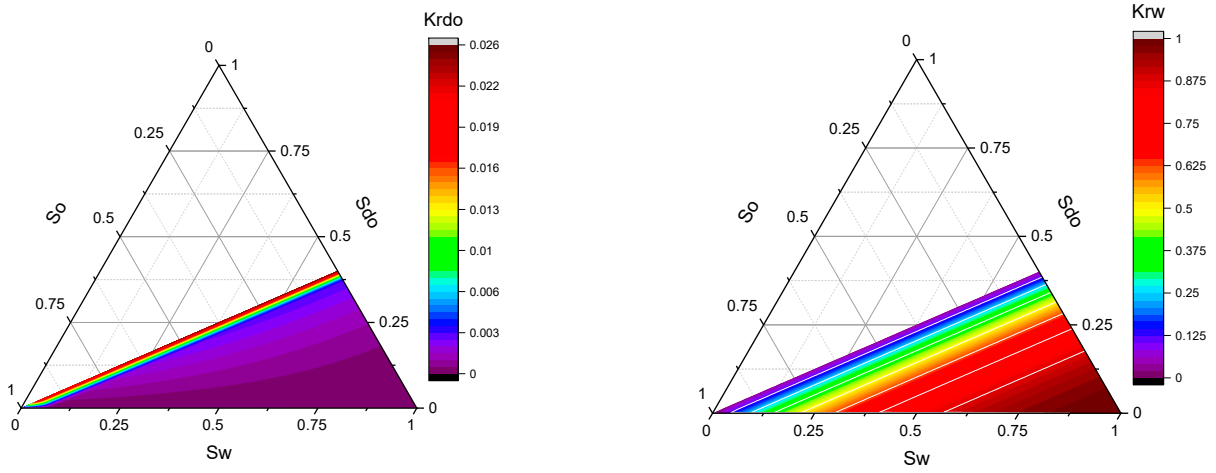

(**a**) (**b**)

Figure 10. The relative permeability ternary diagrams of dispersed oil and continuous water phase when $\phi_d = 0.4$, $\lambda = 0.9$, and $Ca = 10^{-4}$. (**a**) Dispersed oil; (**b**) continuous water.

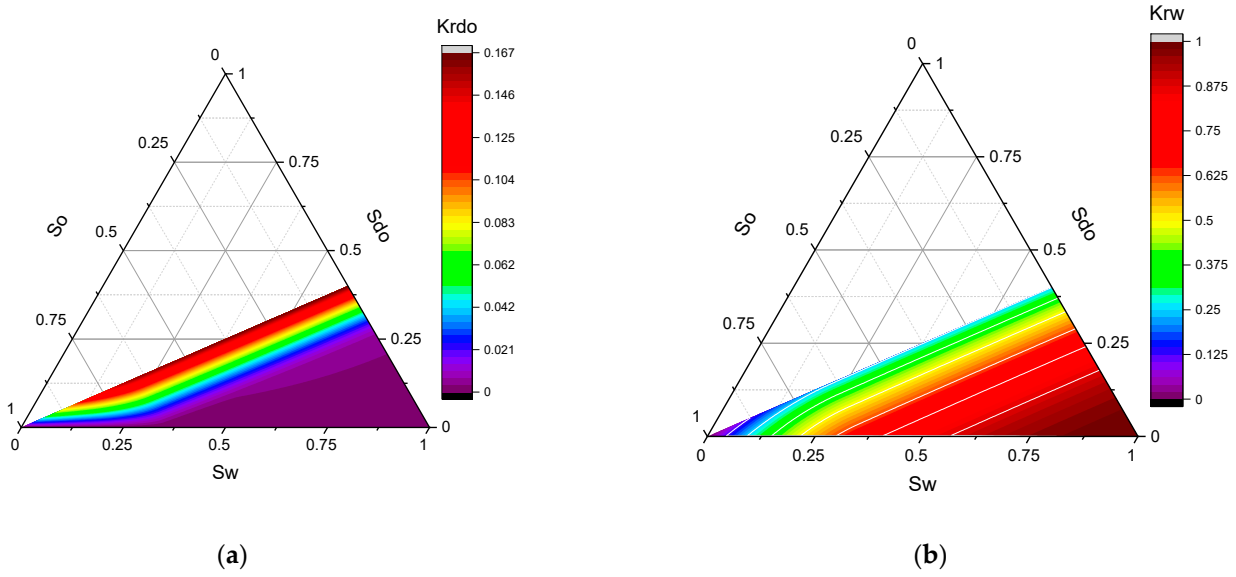

Figure 11. The relative permeability ternary diagrams of dispersed oil and continuous water phase when $\phi_d = 0.4$, $\lambda = 0.6$, and $Ca = 10^{-3}$. (**a**) Dispersed oil; (**b**) continuous water.

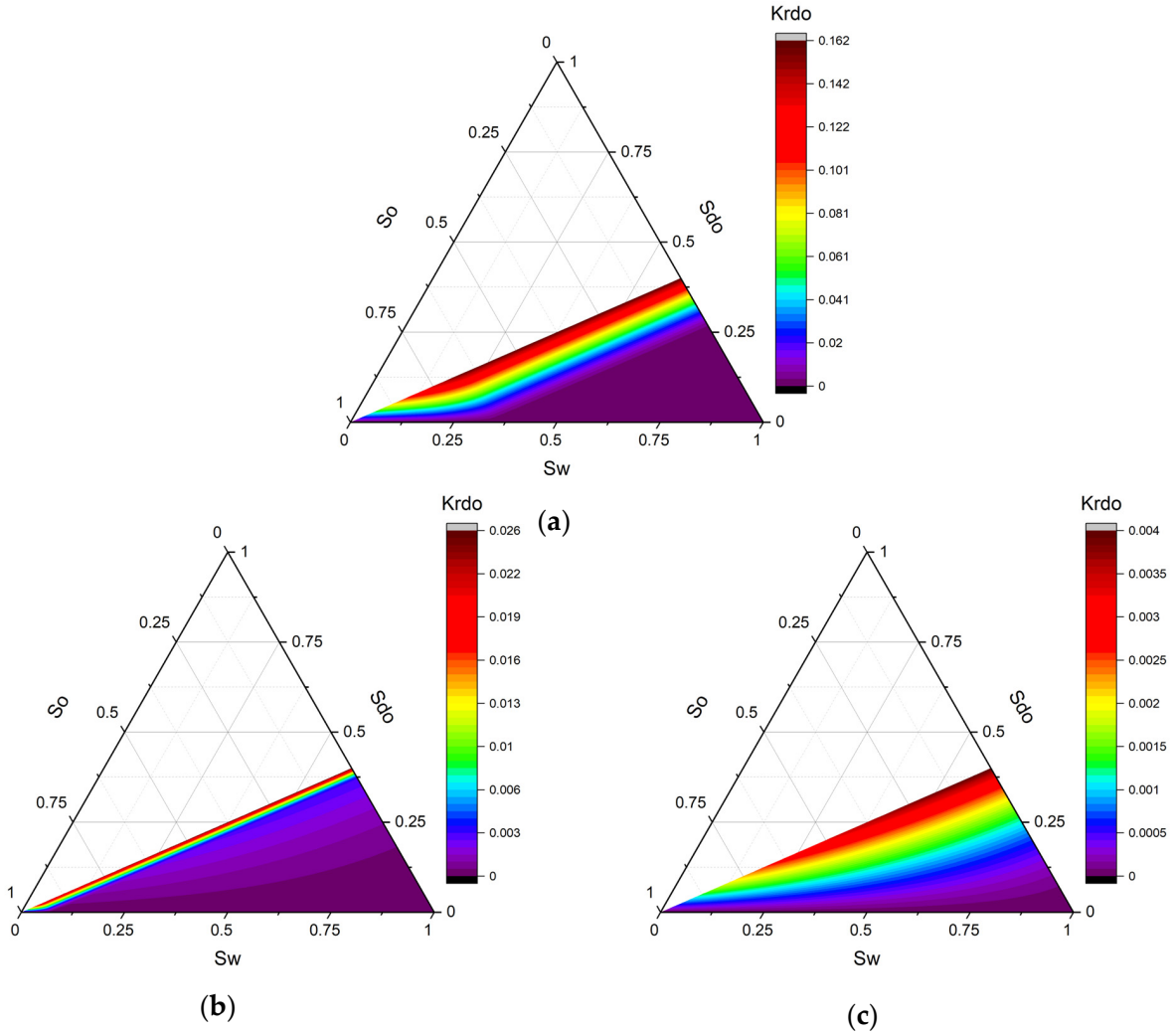

Figure 12. The relative permeability ternary diagrams of the dispersed oil phase with $\phi_d = 0.4$, $Ca = 10^{-4}$, and different λ. (**a**) $\lambda = 0.6$; (**b**) $\lambda = 0.9$; and (**c**) $\lambda = 1.2$.

Figure 13 shows another three diagrams of K_{rdo} with different parameters. Here, we set the volume fraction of the dispersed oil droplets $\phi_d = 0.4$, and the diameter ratio $\lambda = 0.9$. The capillary number Ca of the three diagrams are set to 10^{-3}, 10^{-4}, and 10^{-5}, respectively. The maximum values of three K_{rdo} diagrams are 0.1619, 0.0255, and 0.004, respectively. It is evident that an increase in the capillary number results in a decrease in the resistance encountered by the dispersed phase droplets when passing through the pores, thereby enhancing their ability to pass through the porous medium. A comparison between Figures 12 and 13 reveals that the impact of altering the capillary number on K_{rdo} is significantly more pronounced than that of changing the diameter ratio. In Figure 13, with the fixed parameters $\phi_d = 0.4$ and $\lambda = 0.9$, altering the capillary number Ca leads to an approximate two orders of magnitude variation in the maximum K_{rdo} value, whereas adjusting the diameter ratio λ in Figure 12 does not induce an order of magnitude change in the maximum K_{rdo} value. This observation can be attributed to the fact that the capillary number serves as a parameter governing the capacity of the dispersed phase droplets to pass through the pores when subjected to blockage. Furthermore, under the conditions presented in Figure 13, both ϕ_d and λ are relatively large, signifying that the majority of the dispersed phase droplets experience blocking. As a result, alterations in the capillary number's order of magnitude also provoke corresponding changes in the resistance experienced by the droplets, thereby causing the capillary number to exert a substantial influence on the relative permeability of the dispersed phase droplets.

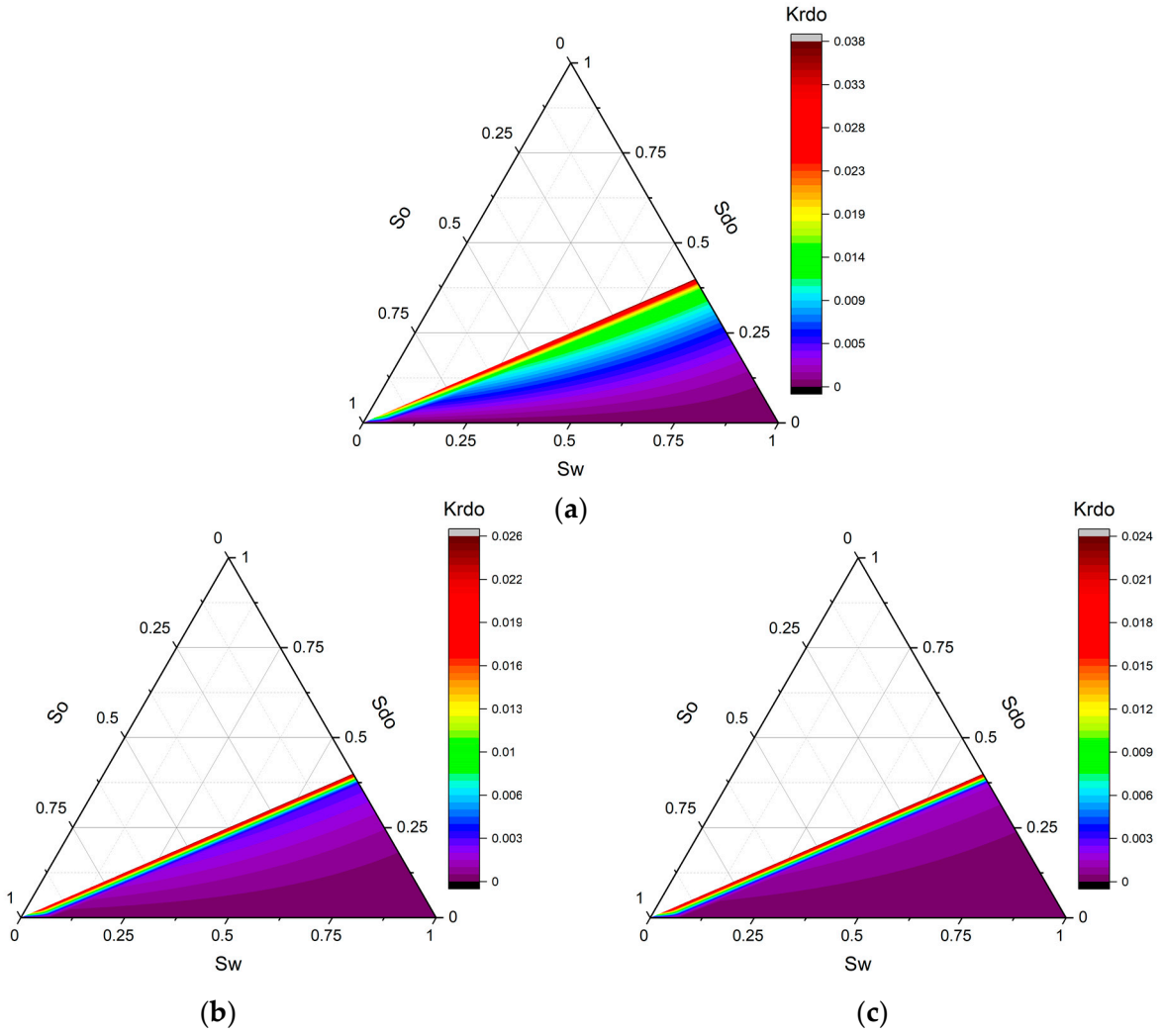

Figure 13. The relative permeability ternary diagrams of the dispersed oil phase with $\phi_d = 0.4$, $\lambda = 0.9$, and different Ca. (**a**) $Ca = 10^{-3}$; (**b**) $Ca = 10^{-4}$; and (**c**) $Ca = 10^{-5}$.

When the value of ϕ_d is relatively small, the area of the ternary diagram of relative permeability decreases. Investigating the effects of various parameters on relative permeability within the ternary diagram becomes less intuitive. Additionally, as seen from the figures mentioned earlier, the growing patterns in the values of K_{rdo} are similar. Consequently, we can substitute the study of endpoint values (the maximum value of K_{rdo}) under different conditions for the entire ternary diagram of relative permeability.

Table 1 is a table of K_{rdo} endpoint values under different parameter scenarios. As evident in the table, the capillary number ca exhibits a more substantial impact on the maximum value of K_{rdo} compared to the diameter ratio lambda, as previously highlighted. When assessing the influence of ϕ_d on the relative permeability of the dispersed oil droplets, it is essential to note that ϕ_d serves as the upper boundary for S_{do} values. In other words, ϕ_d signifies the carrying capacity of dispersed oil droplets within the continuous water phase. When the ratio of S_{do} to S_w equals ϕ_d, it implies a uniform distribution of oil droplets within the emulsion, as dispersed oil droplets participate in all flow channels occupied by the continuous water phase. This corresponds to values of the diagonal line in the ternary phase diagram. Conversely, when the ratio of S_{do} to S_w is less than ϕ_d, it suggests that the water flow region can be partitioned into an emulsion flow domain and a purely continuous water flow domain. Consequently, dispersed oil droplets only participate in the flow of specific channels, thereby diminishing their capacity to pass through the pore spaces. By analyzing the maximum values of K_{rdo} at varying ϕ_d values, as well as their ratio, it becomes apparent that the actual ability of dispersed oil droplets to pass through pores weakens, despite the increase in the maximum value of K_{rdo} as ϕ_d increases. We can consider the case when $\lambda = 1.2$ and $Ca = 10^{-3}$, and take the maximum value of K_{rdo}/ϕ_d as an example. It can be observed that when ϕ_d = 0.1, 0.2, and 0.4, the maximum values of K_{rdo}/ϕ_d are 0.605, 0.538, and 0.403, respectively, showing a decreasing trend when ϕ_d increases. Based on Darcy's law for multiphase flow, an increase in K_{rdo}/ϕ_d implies that a larger pressure drop is required for the dispersed oil droplets to pass through at the same mass flow rate. Examined from a microscopic perspective, the probability of individual dispersed oil droplets passing through pores decreases, even though the aggregate volume of dispersed oil droplets passing through pores escalates. Statistically, this phenomenon is readily understandable, given that the likelihood of droplets becoming trapped in pores becomes larger as the volume fraction of dispersed oil droplets augments.

Table 1. K_{rdo} endpoint values with different dimensionless parameters.

	ϕ_d=0.1			ϕ_d=0.2			ϕ_d=0.4		
	$\lambda = 0.6$	$\lambda = 0.9$	$\lambda = 1.2$	$\lambda = 0.6$	$\lambda = 0.9$	$\lambda = 1.2$	$\lambda = 0.6$	$\lambda = 0.9$	$\lambda = 1.2$
$Ca = 10^{-3}$	0.0649	0.0611	0.0605	0.1123	0.1081	0.1075	0.1663	0.1619	0.1613
$Ca = 10^{-4}$	0.0249	0.0148	0.0133	0.0315	0.0202	0.0186	0.0374	0.0255	0.0239
$Ca = 10^{-5}$	0.0167	0.0038	0.002	0.0182	0.0039	0.002	0.0191	0.004	0.002

Concerning the relationship between the relative permeability of dispersed phase droplets and the three saturation parameters, observations can be made from Figures 8–10. Generally, when considering a fixed value of S_o/S_w, as S_{do} approaches its upper limit ϕ_d, the growth rate of K_{rdo} accelerates. When considering a fixed value of S_{do}, an increase in the S_o/S_w ratio results in a decline in K_{rdo} values.

To briefly summarize, among the three dimensionless numbers ϕ_d, λ and Ca, the variation of Ca has the most substantial impact on the relative permeability of dispersed phase droplets. This implies that reducing interfacial tension and increasing the injection pressure are vital ways to improve the permeability of dispersed phase droplets. Increases in both ϕ_d and λ contribute to a reduction in the relative permeability of dispersed phase droplets. It is worth mentioning that in experiments and chemical oil reservoir development, ϕ_d and λ are usually not independent parameters but are closely related to the physicochemical properties of the reservoir and surfactants. Nevertheless, in this theoretical investigation,

these two parameters are provisionally regarded as independent, and their impacts on the flow performance of emulsions are analyzed. In practical reservoir development, it is crucial to distinguish the sources of dispersed phase droplets (whether pre-prepared or in situ generated) and adjust these dimensionless numbers accordingly, to attain the desired relative permeability.

6. Conclusions

A novel relative permeability model applicable to heavy oil chemical flooding emulsion systems is presented in this study. The emulsion system is considered as an O/W emulsion and comprises three phases: continuous oil phase, continuous water phase, and dispersed oil phase. The new relative permeability model takes the physicochemical properties of emulsions and the properties of porous media into account, as well as the interactions between dispersed phase droplets and pores. The validity of the relative permeability model is verified through a sandpack emulsion displacement experiment. The dimensionless numbers determining the relative permeability of dispersed phase droplets are analyzed. The following conclusions are drawn from this study:

1. The emulsion flow behavior through a single capillary was carefully investigated. The flow of emulsion in the capillary, based on the relative size of dispersed phase droplets and the capillary, was divided into three types: (a) the droplet size and capillary diameter are similar; (b) the droplet size is much smaller than capillary diameter; (c) the droplet size is larger than the capillary diameter.

2. The real reservoir is considered as a series of capillary bundles with diameters following the PSD (pore size distribution) function. Assuming the reservoir is hydrophilic, a calculation model for the three-phase relative permeability of the O/W emulsion system was established, by classifying different-sized capillaries as occupied by different fluids. A more realistic log-normal PSD function was used, instead of using the simplified uniform diameter, when calculating relative permeability.

3. A sandpack emulsion displacement experiment was used to verify the effectiveness of the proposed relative permeability model. The experiment process was injecting a pre-prepared emulsion into a sandpack saturated with oil. The injection was at a constant flow rate of 0.5 mL/min. The volume fraction of the dispersed oil phase in the pre-prepared emulsion was 0.2. Based on a one-dimensional three-phase numerical simulator, the simulated cumulative emulsion production using the proposed relative permeability model showed good consistency with the experimental data. The maximum error in the cumulative production did not exceed 10%. Therefore, the new relative permeability model is suitable for the numerical simulation of heavy oil emulsion three-phase systems.

4. Three dimensionless numbers related to the emulsion porous flow process, ϕ_d, λ, and Ca, were proposed. The effects of these three dimensionless numbers on the relative permeability of dispersed oil droplets were analyzed. The capillary number Ca exerts the most significant influence on the relative permeability among the dimensionless parameters. Alterations in the order of magnitude of Ca correspond to concomitant changes in the order of magnitude for the relative permeability of the dispersed phase. The increase in diameter ratio λ and dispersed phase volume fraction ϕ_d will reduce the ability of the dispersed phase to pass through porous media. The newly developed three-phase relative permeability model offers valuable insights for enhancing the understanding and prediction of emulsion flow behavior.

Author Contributions: Z.S.: Manuscript writing, Conceptualization, Investigation, Methodology. K.Z.: Experimental studies, Validation. Y.D.: Methodology, Supervision. All authors have read and agreed to the published version of the manuscript.

Funding: This research was funded by the National Key Research and Development Program of China (Grant No. 2018YFA0702400).

Data Availability Statement: All the data supporting this study can be found in the manuscript.

Conflicts of Interest: The authors declare no conflict of interest.

Nomenclature

Nomenclature			
b	Water film thickness of deformed oil droplets in a capillary tube, μm	Q	Flow rate of the porous medium, m^3/s
d_e	Average diameter of dispersed emulsion droplets, μm	R	Radius of capillary tube, μm
n	Exponent of power law PSD function	$\overline{R}$	Mean radius of log-normal PSD function, 10^{-7} m
p	Fluid pressure, kPa	S_{do}	Saturation of dispersed oil phase
q_e	Total flow rate of emulsion flow in a single capillary tube, m^3/s	S_o	Saturation of continuous oil phase
q_0	Flow rate of single-phase fluid in a single capillary tube, m^3/s	S_w	Saturation of continuous water phase
r	Radical coordinate, m	U	Dimensionless velocity of droplets
r_{eff}	Effective radius of small droplets suspension, μm	V	Dimensionless average velocity in capillary
v'	Dimensionless velocity	**Greek symbols**	
z	Axial coordinate, m	β	Ratio of distance between neigh-boring spheres to tube radius
A	Cross area of the porous medium, m^2	μ	Viscosity of the fluid, mPa·s
Ca	Capillary number	μ_o	Oil viscosity, mPa·s
G_{V_0}	Additional pressure drop coefficient	μ_w	Water viscosity, mPa·s
K	Permeability of the porous medium, mD	λ	Ratio of droplets diameter to capillary diameter
K_{rdo}	Relative permeability of dispersed oil phase	ϕ_d	Dispersed phase volume fraction
K_{ro}	Relative permeability of continuous oil phase	ω	Ratio of oil viscosity to water viscosity
K_{rw}	Relative permeability of continuous water phase	ξ	Resistance factor of emulsion flow
L	Length of the porous medium, m	ϕ	Porosity of the porous medium
$\boldsymbol{P'}$	Dimensionless pressure	σ	Standard deviation of log-normal PSD function
P_c	Capillary pressure, kPa	σ_0	Interfacial tension, mN/m
ΔP	Pressure drop along the capillary tube, kPa	θ	Contact angle between the non-wetting phase and the pore
$\Delta P'_{drop}$	Dimensionless pressure drop per droplet in capillary		

References

1. Guo, K.; Li, H.; Yu, Z. In-situ heavy and extra-heavy oil recovery: A review. *Fuel* **2016**, *185*, 886–902. [CrossRef]
2. Nagatsu, Y.; Abe, K.; Konmoto, K.; Omori, K. Chemical Flooding for Enhanced Heavy Oil Recovery via Chemical-Reaction-Producing Viscoelastic Material. *Energy Fuels* **2020**, *34*, 10655. [CrossRef]
3. Santos, R.G.; Loh, W.; Bannwart, A.C.; Trevisan, O.V. An overview of heavy oil properties and its recovery and transportation methods. *Braz. J. Chem. Eng.* **2014**, *31*, 571–590. [CrossRef]
4. Zhou, X.; Yuan, Q.; Peng, X.; Zeng, F.; Zhang, L. A critical review of the CO_2 huff 'n' puff process for enhanced heavy oil recovery. *Fuel* **2018**, *215*, 813–824. [CrossRef]
5. Dong, M.; Ma, S.; Liu, Q. Enhanced heavy oil recovery through interfacial instability: A study of chemical flooding for Brintnell heavy oil. *Fuel* **2009**, *88*, 1049–1056. [CrossRef]
6. Lamas, L.; Botechia, V.; Schiozer, D.; Rocha, M.; Delshad, M. Application of polymer flooding in the revitalization of a mature heavy oil field. *J. Pet. Sci. Eng.* **2021**, *204*, 108695. [CrossRef]
7. Liu, Q.; Dong, M.; Ma, S.; Tu, Y. Surfactant enhanced alkaline flooding for Western Canadian heavy oil recovery. *Colloids Surfaces A Physicochem. Eng. Asp.* **2007**, *293*, 63–71. [CrossRef]
8. Panthi, K.; Weerasooriya, U.; Mohanty, K.K. Enhanced recovery of a viscous oil with a novel surfactant. *Fuel* **2020**, *282*, 118882. [CrossRef]
9. Wei, J.; Li, J.; Shi, X.; Zhou, R. Combination of alkali–surfactant–polymer flooding and horizontal wells to maximize the oil recovery for high water cut oil reservoir. *Energy Rep.* **2021**, *7*, 5955–5964. [CrossRef]
10. Druetta, P.; Raffa, P.; Picchioni, F. Chemical enhanced oil recovery and the role of chemical product design. *Appl. Energy* **2019**, *252*, 113480. [CrossRef]
11. Ahmadi, M.; Chen, Z. Challenges and future of chemical assisted heavy oil recovery processes. *Adv. Colloid Interface Sci.* **2019**, *275*, 102081. [CrossRef] [PubMed]
12. Kar, T.; Hascakir, B. Effect of solvent type on emulsion formation in steam and solvent-steam flooding processes for heavy oil recovery. *Colloids Surfaces A Physicochem. Eng. Asp.* **2021**, *611*, 125783. [CrossRef]
13. Uzoigwe, A.C.; Marsden, S.S., Jr. Emulsion Rheology and Flow through Unconsolidated Synthetic Porous Media. In Proceedings of the Fall Meeting of the Society of Petroleum Engineers of AIME, Houston, TX, USA, 4–7 October 1970. Volume All Days, SPE-3004-MS. [CrossRef]
14. McAuliffe, C.D. Oil-in-Water Emulsions and Their Flow Properties in Porous Media. *J. Pet. Technol.* **1973**, *25*, 727–733. [CrossRef]
15. Soo, H.; Radke, C.J. Flow mechanism of dilute, stable emulsions in porous media. *Ind. Eng. Chem. Fundam.* **1984**, *23*, 342–347. [CrossRef]

16. Khambharatana, F.; Thomas, S.; Ali, S.M.F. Macroemulsion Rheology and Drop Capture Mechanism During Flow in Porous Media. In Proceedings of the SPE International Oil and Gas Conference and Exhibition in China, Beijing, China, 2–6 November 1998. Volume All Days, SPE-48910-MS. [CrossRef]
17. Alvarado, D.; Marsden, S.J. Flow of Oil-in-Water Emulsions through Tubes and Porous Media. *Soc. Pet. Eng. J.* **1979**, *19*, 369–377. [CrossRef]
18. Wang, F.; Qu, Z.; Xue, Z. A study on emulsion flow in porous media with micromodel. *J. Northwestern Univ.* **2003**, *33*, 603–607.
19. Abou-Kassem, J.; Ali, S.F. Modeling of Emulsion Flow In Porous Media. *J. Can. Pet. Technol.* **1995**, *34*, PETSOC-95-06-02. [CrossRef]
20. Devereux, O.F. Emulsion flow in porous solids: II. experiments with a crude oil-in-water emulsion in porous sandstone. *Chem. Eng. J.* **1974**, *7*, 129–136. [CrossRef]
21. Yu, L.; Ding, B.; Dong, M.; Jiang, Q. A new model of emulsion flow in porous media for conformance control. *Fuel* **2019**, *241*, 53–64. [CrossRef]
22. Ding, B.; Dong, M.; Yu, L. A model of emulsion plugging ability in sandpacks: Yield pressure drop and consistency parameter. *Chem. Eng. Sci.* **2019**, *211*, 115248. [CrossRef]
23. Soo, H.; Radke, C. A filtration model for the flow of dilute, stable emulsions in porous media—I. *Theory. Chem. Eng. Sci.* **1986**, *41*, 263–272. [CrossRef]
24. Xuewen, L.; Wanli, K. Advances in crude oil emulsion stability and interfacial film. *Oil-Gas Field Surf. Eng.* **2003**, *22*, 7–8.
25. Wei, B.; Hou, J.; Sukop, M.C.; Du, Q.; Wang, H. Flow behaviors of emulsions in constricted capillaries: A lattice Boltzmann simulation study. *Chem. Eng. Sci.* **2020**, *227*, 115925. [CrossRef]
26. Bear, J. Dynamics of Fluids in Porous Media. *Soil Sci.* **1975**, *120*, 162–163. [CrossRef]
27. Wang, H.; Skalak, R. Viscous flow in a cylindrical tube containing a line of spherical particles. *J. Fluid Mech.* **1969**, *38*, 75–96. [CrossRef]
28. Thomas, H. The wall effect in capillary instruments: An improved analysis suitable for application to blood and other particulate suspensions. *Biorheology* **1962**, *1*, 41–56. [CrossRef]
29. Hodges, S.R.; Jensen, O.E.; Rallison, J.M. The motion of a viscous drop through a cylindrical tube. *J. Fluid Mech.* **2004**, *501*, 279–301. [CrossRef]
30. Bowen, W.; Welfoot, J.S. Modelling of membrane nanofiltration—Pore size distribution effects. *Chem. Eng. Sci.* **2002**, *57*, 1393–1407. [CrossRef]
31. Yang, Y.; Liu, P.; Zhang, W.; Liu, Z.; Sun, H.; Zhang, L.; Zhao, J.; Song, W.; Liu, L.; An, S.; et al. Effect of the Pore Size Distribution on the Displacement Efficiency of Multiphase Flow in Porous Media. *Open Phys.* **2016**, *14*, 610–616. [CrossRef]
32. Zhai, Q.; Rahardjo, H.; Satyanaga, A. A pore-size distribution function based method for estimation of hydraulic properties of sandy soils. *Eng. Geol.* **2018**, *246*, 288–292. [CrossRef]